Complexes of the Bis(di-tert-butyl-aniline)amine Pincer Ligand: The Case of Copper

Nicolas Leconte, Solène Gentil, Florian Molton, Christian Philouze, Alan Le Goff, Fabrice Thomas

EurJIC
European Journal of Inorganic Chemistry

Full Paper
doi.org/10.1002/ejic.202000379

Redox Noninnocent Ligands

Complexes of the Bis(di-*tert*-butyl-aniline)amine Pincer Ligand: The Case of Copper

Nicolas Leconte,*[a] Solène Gentil,[a,b] Florian Molton,[a] Christian Philouze,[a] Alan Le Goff,*[a] and Fabrice Thomas*[a]

Abstract: The *N*,*N*-bis(2-amino-3,5-di-*tert*-butylphenyl)amine pincer ligand was coordinated to copper. Depending on the copper source, a mononuclear complex $\mathbf{1}^+$ or a trimer **2** could be isolated and were structurally characterized. Complex $\mathbf{1}^+$ consists of two deprotonated iminobenzoquinone ligands coordinated to a Cu(I) center. Complex **2** is trinuclear with a (3:3) (M:L) stoichiometry, featuring a three-fold repetition of a unit made of a Cu(II) center coordinated to a tridentate ligand radical-dianion. In **2**, the metal ions are bridged by an anilido nitrogen. The coordination sphere of each copper is completed to four by a neighboring iminosemiquinone moiety. Complex $\mathbf{1}^+$ belongs to an electron-transfer series. The paramagnetic complexes **1** and $\mathbf{1}^{2+}$ were generated and characterized by EPR and Vis-NIR spectroscopy. Complex **1** exhibits an isotropic resonance at g = 2.00, which is reminiscent of Cu(I) iminosemiquinone species. The dication $\mathbf{1}^{2+}$ exhibits a metal-based ground spin state and hence is described as a Cu(II) iminobenzoquinone complex. Both **1** and $\mathbf{1}^+$ show a NIR band (954, 980 nm) of high intensity (> 20 $mM^{-1}\,cm^{-1}$) assigned to ligand-based charge transfer transitions. Two-electron reduction of **1** produces **2** via ligand release and disproportionation. Conversely, oxidation of **2** affords $\mathbf{1}^+$. Finally, carbon-nanotube-supported complex **2** is active towards electrocatalytic reduction of H_2O_2.

Introduction

Redox noninnocent ligands constitute a fascinating class of chelators whose spectroscopic, chemical, magnetic and coordination properties can be modulated by external redox stimuli.[1] The corresponding complexes find applications in number of fields, including optics,[1c] magnetism,[1e,1h] catalysis.[1a,1b,1d,1f,1h] The N_2O chelate N,N-bis(3,5-di-*tert*-butyl-2-phenoxide)amide (H_3L^O) is one of the most richly studied redox noninnocent ligands. This pincer ligand was originally designed by Balch and Girgis during the 70's,[2] and was extensively studied by Pierpont and other groups.[3] Its tridentate nature makes it a versatile ligand, capable of coordinating metals of the d-block,[2,3,3h–3j,3l,3n,3p–3s] f-block[3k,3r] as well as post-transition elements.[3g,3m,3o,3r] Once engaged in coordination in its partially or fully deprotonated form, it was demonstrated to produce persistent radicals, which could be characterized and even crystallized. Amongst the many metals investigated the cobalt ion[3a,3c,3d,3l] and to a lesser extend the zinc ion[3i] were shown to promote valence tautomerism phenomena: In the first case an electron redistribution is observed between the metal and the ligand as a function of the temperature, whereas in the latter case the redistribution occurs between the ligands. Another metal of great interest is copper since a related copper-radical unit could be identified in the active site of an enzyme, galactose oxidase.[4] In this biomimetic context Wieghardt et al. demonstrated that the pincer ligand H_3L^{O}[3j] as well as related architectures[5] could be used to prepare functional models of the enzyme.

We recently described the N_3 chelate analog of H_3L^O, namely H_3L^N[6a] and investigated its coordination chemistry with several transition metal ions (Scheme 1).[6,7] The easier oxidation of anilines compared to phenols allowed us to prepare complexes with unprecedented oxidation states. As an example, a bench stable octahedral Mn^V radical species ($[Mn^V(L^N_{IBQ})(L^N_{ISQ})]^{2+}$, could be isolated and even crystallized. By X-ray diffraction we established that the ligand coordinates in a tridentate fashion in $[Mn^V(L^N_{IBQ})(L^N_{ISQ})]^{2+}$.[6a] Our previous work also highlighted that H_3L^N can behave as a bidentate ligand after reaction with group 10 metal ions, leading to complexes of general formula $[M^{II}(HL^N_{ISQ})_2]$.[6b] These species feature an uncoordinated pending NH_2 residue, offering an anchoring fragment or a proton relay for further catalytic applications.

Herein the coordination chemistry of H_3L^N is further investigated with copper. In agreement with our expectations, the N_3 ligand offers unique properties, distinct from that of H_3L^O. Two complexes of distinct M:L ratio (1:2 and 3:3) were isolated as

[a] *Dr. N. Leconte, Dr. S. Gentil, F. Molton, Dr. C. Philouze, Dr. A. Le Goff, Prof. F. Thomas*
Univ. Grenoble Alpes,
CNRS, DCM, 38000 Grenoble, France
E-mail: Nicolas.Leconte@univ-grenoble-alpes.fr
alan.le-goff@univ-grenoble-alpes.fr
Fabrice.Thomas@univ-grenoble-alpes.fr
[b] *Dr. S. Gentil*
Univ. Grenoble Alpes,
CEA, CNRS, Laboratoire de Chimie et Biologie des Métaux,
38000 Grenoble, France
Supporting information and ORCID(s) from the author(s) for this article are available on the WWW under https://doi.org/10.1002/ejic.202000379.
This manuscript is part of the Special Collection Pincer Chemistry and Catalysis.

Full Paper
doi.org/10.1002/ejic.202000379

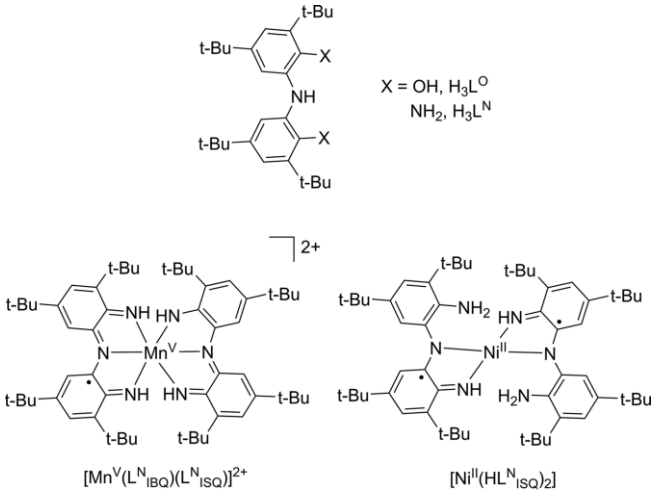

Scheme 1. Structure of the ligands H_3L^O and H_3L^N as well as previously reported complexes of H_3L^N.[6]

crystals (complexes $\mathbf{1}^+$ and **2**, respectively). We demonstrate that an interconversion can be triggered by controlled electron transfer. We disclose that complex $\mathbf{1}^+$ belongs to an electron transfer series and establish the electronic structure of each member by spectro-electrochemistry combined with DFT calculations. Furthermore, the electrocatalytic activity of carbon-nanotube-supported complex **2** towards H_2O_2 activation was assessed in water.

Results and Discussion

Synthesis

We described the synthesis of the ligand H_3L^N in previous work.[6a] The copper radical species were tentatively prepared from $CuCl_2$, using a classical protocol, i.e. refluxing a solution of H_3L^N (2 molar equiv.) and the metal ion (1 molar equiv.) in the presence of a base (4 molar equiv.) Such a strategy proved to be efficient for Mn, Co and group 10 metal complexes.[6,7] Unfortunately, the isolation of any Cu-containing compound failed under identical conditions (methanolic solution). Finally, the addition of $KSbF_6$ to the reaction mixture was the key parameter to observe the precipitation of a finely divided crystalline powder. The isolated complex ($\mathbf{1}^+(SbF_6^-)$, see below) was found to be diamagnetic at r.t., with a ^1H NMR spectrum displaying resonances in the range 7.83–1.12 ppm. As demonstrated below it is a Cu(I) complex, showing that a redox reaction occurred between the ligand in overstoichiometry and the metal. Complex $\mathbf{1}^+(SbF_6^-)$ shows three distinct N–H stretching bands at 3528, 3417, 3379 cm^{-1}.

Complex **2** was prepared by refluxing equimolar amounts of the copper(I) salt $[Cu(CH_3CN)_4]$ (PF_6^-) and H_3L^N, in acetonitrile. An excess of NEt_3 was added to enforce full deprotonation of the ligand. Similarly to $\mathbf{1}^+(SbF_6^-)$, complex **2** is diamagnetic, as demonstrated by ^1H NMR in CD_2Cl_2. Its IR spectrum however shows only two N–H stretchings at 3361 and 3317 cm^{-1}, suggesting a different oxidation/protonation state of the ligand within **2**. Strikingly, complex **2** was found to be a Cu(II) complex, revealing an subtle control of the redox reaction between the ligand and the metal by the reaction conditions.

X-ray Crystal Structures

Complex $\mathbf{1}^+(SbF_6^-)$ was crystallized by vapor diffusion at r.t. of MeOH into a benzene solution of the compound, while complex **2** was crystallized by vapor diffusion at r.t. of MeCN into a benzene solution of the complex. Their crystal structures are depicted in Figure 1. The quality of the structure of $\mathbf{1}^+(SbF_6^-)$ (Figure 1a) was found to be lower than that of **2** due to twin, resulting in significant standard deviations of the bonds within the ligands. The crystal structure contains two distinct molecules A and B, which both show a tetra-coordinated copper ion. The geometry of the central metal ion is intermediate between square planar and tetrahedral, with a τ_4 index of 0.39–0.42 (0 for a square plane, 1 for a tetrahedron),[8] as observed in the homoleptic 1:2 (Cu:L) complex of the 2-(2-thiomethyl)anilino-4,6-di-*tert*-butylphenol.[9] The copper center is chelated by two ligands, which coordinate in a bidentate fashion by the N1A/B, N2A/B, N4A/B and N5A/B atoms (Figure 1, Table 1). One terminal amino group of each ligand (N3A/B and N6A/B) remains pending under its NH_2 form. Interestingly, the NH_2 groups of the two ligands adopt a *cis* configuration, in sharp contrast with $[Ni^{II}(HL^{N\cdot})_2]$, whereby they lie in *trans* configuration.[6b] Both NH_2 groups point almost orthogonal to the Cu,N1,N2,N4,N5 plane and subsequently on the same side of the complex. The SbF_6^- counterion is located above the copper ion and interacts through hydrogen bonding with both pending NH_2 (shortest F–N distance 2.95(1)-3.45(1) Å). The C1–N1 and opposite C13–N4 bond lengths are short (1.28(1)-1.31(1) Å) and mainly correspond to double bonds. The neighboring C2–N2 and C14–N5 are also relatively short (1.31(1)-1.34(1) Å), which altogether support a neutral HL^N_{IBQ} formulation of both

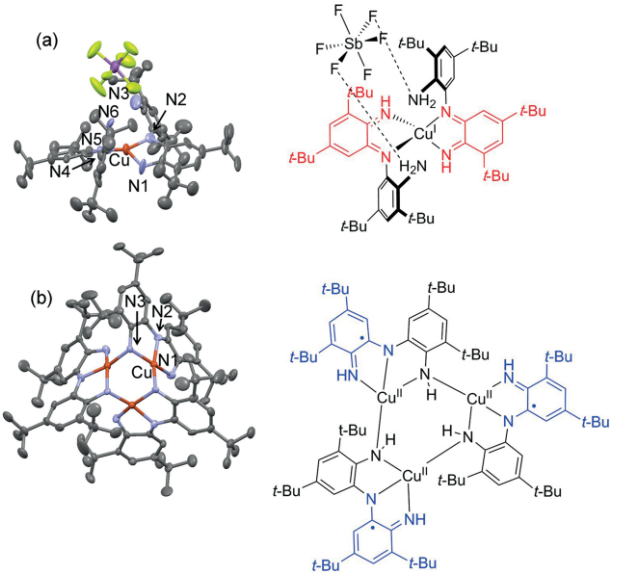

Figure 1. ORTEP (30 % probability level) and schematized views of complexes (a) $\mathbf{1}^+(SbF_6^-)$ and (b) **2**. The hydrogen atoms are omitted for clarity in the ORTEP views.

Full Paper
doi.org/10.1002/ejic.202000379

ligand molecules.[6b,10] Hence, a (+I) oxidation state of the copper is expected, which is consistent with tetrahedral distortion at the metal center.

Table 1. Selected bond lengths in $\mathbf{1}^+$ and **2**.[a]

Bond length	$\mathbf{1}^+$	**2**	Bond length	$\mathbf{1}^+$	**2**
Cu1–N1	1.906(8) 1.918(9)	1.937(7) 1.899(7) 1.947(9)	Cu1–N5	1.945(8) 1.976(7)	–
Cu1–N2	1.977(7) 1.967(7)	1.930(9) 1.925(9) 1.941(8)	Cu1–N3′	–	1.99/1.97(1) 1.98(1) 1.94(1)
Cu1–N3	–	1.972(8) 1.965(6) 1.958(9)	Cu1–Cu1	–	2.92(1) 2.91(1) 2.88(1)
Cu1–N4	1.894(7) 1.919(9)	–			

[a] In Å. More than one value indicated means that distinct molecules are present in the crystal cell.

The structure of **2** shows a trinuclear copper complex of stoichiometry Cu:L (3:3). Three independent molecules A, B and C are present, whose structures do not differ significantly. Each copper center is four-coordinate, bound to the N1, N2, N3 of one ligand and the N3′ atom of a different ligand. Hence all the N3 atoms act as μ-anilido bridges. The copper ion is less tetrahedrally distorted than in $\mathbf{1}^+$, as judged by the τ_4 index of 0.24–0.28. The C1–N1 bond length is 1.32(1) Å, while the C7–N3 one is 1.42(1)-1.44(1) Å, indicative of distinct oxidation states for each aniline counterpart within a ligand. The C1–N1 bond length is close to that measured in $[Ni(HL^{N\bullet})_2]$ and $[Pt(HL^{N\bullet})_2]$ (1.339 Å), supporting an iminosemiquinone description of each non-bridging ring.[6b,7,10] The other (bridging) rings show anilido features, which is demonstrated by the significant displacement (average 0.58 Å) of the N3 atom above the Cu–C7–Cu cores that contrasts with the expected planarity for a nitrido (N^-) or iminosemiquinone binding. One consequence is the chair conformation of the Cu1–N3–Cu1′–N3′–Cu1″–N3″ core. Finally the intermetallic distance is 2.88(1)-2.92(1) Å, which is in the expected range for doubly bridged copper(II) μ-phenolato dimers,[11] further supporting the (+II) oxidation of the metal ions within **2**.

Electrochemistry

The electrochemical behaviour of $\mathbf{1}^+$ and **2** has been investigated in CH_2Cl_2 containing tetra-*n*-butylammonium perchlorate (TBAP) as supporting electrolyte. The cyclic voltammetry (CV) curves recorded under Ar (glove box) are depicted in Figure 2, while the potentials given relative to the Fc^+/Fc reference are summarized in Table 2.

The CV of complex $\mathbf{1}^+$ shows four redox events in the potential range –2 to 1 V (Figure 2a, Scheme 2 and Scheme 3). Two reversible reduction waves are observed at $E_{1/2}^{red1}$ = –0.75 and $E_{1/2}^{red2}$ = –1.43 V, which correspond to two successive $HL^N_{IBQ}/(HL^N_{ISQ})^-$ redox couples. The first oxidation wave is characterized by a large peak separation (E_p^{a1} = 0.29, E_p^{c1} = –0.15 V), which demonstrates that oxidation is accompanied by a large

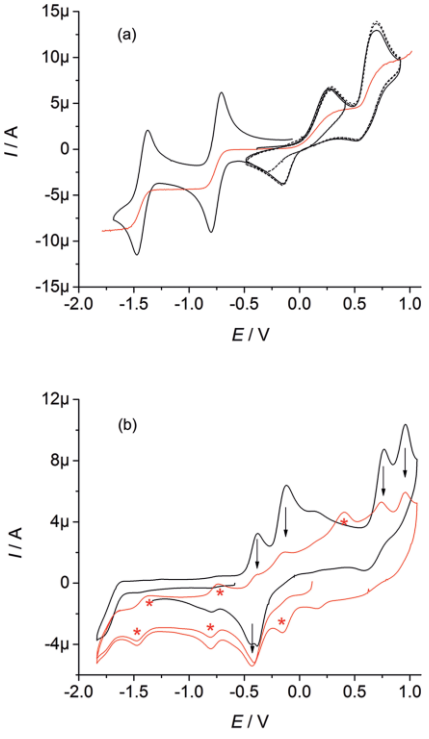

Figure 2. CV curve of (a, black) $\mathbf{1}^+$ and (b, black) **2** in a 0.5 mM CH_2Cl_2 solution containing 0.1 M TBAP at a carbon electrode. The red line in a) represents the RDE curve, the red line in b) the CV curve of complex **2** after electrolysis at 0.2 V. The red stars denotes the features of complex $\mathbf{1}^+$, the black arrows denote the features of complex **2**. Scan rate, 0.1 V/s; T, 298 K; ref. Fc^+/Fc.

Table 2. Electrochemical properties of the complexes.[a]

Complex	$E_{1/2}^{red2}$	$E_{1/2}^{red1}$	$E_{1/2}^{ox1}$ [b]	E_p^{a2}	E_p^{a3}	E_p^{a4}
$\mathbf{1}^+$	–1.43	–0.75	0.06	0.70	–	–
2	–	–	–0.40	–0.13	0.78	0.97

[a] In CH_2Cl_2 containing 0.1 M TBAP. All the potentials are given in V, relative to Fc^+/Fc reference. [b] Calculated as the average between E_p^{a1} et E_p^{c1}. The ΔE is 0.44 V for $\mathbf{1}^+$ because of structural rearrangements (see the text).

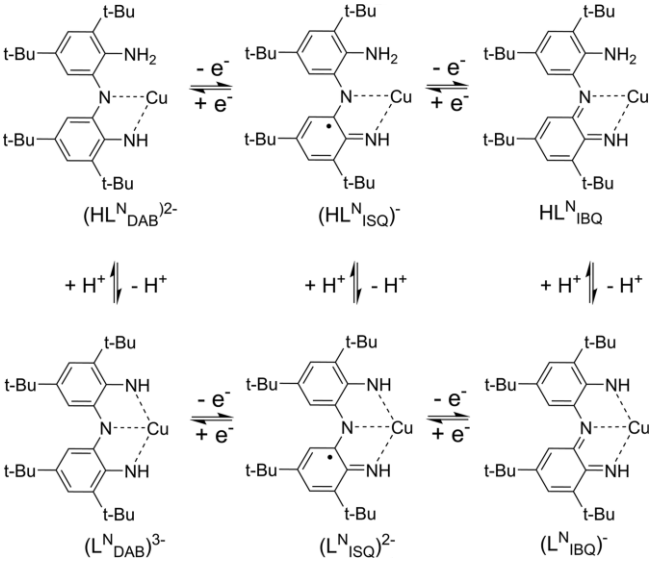

Scheme 2. Relevant oxidation and protonation states with nomenclature for H_3L^N once coordinated to copper.

reorganization of the complex. Hence we assign this wave to a metal-centered redox event, whereby the tetrahedrally distorted Cu(I) center is oxidized into a square pyramidal Cu(II) center (see below). The second oxidation wave is irreversible and occurs at E_p^{a2} = 0.70 V. It is tentatively assigned to the oxidation of one pending aniline moiety.

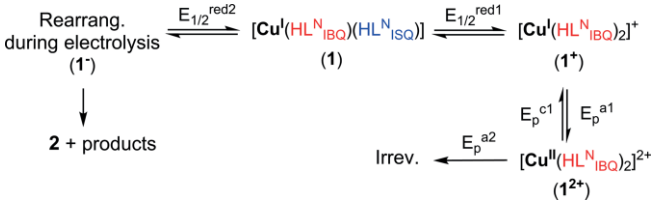

Scheme 3. Redox chemistry of complex $\mathbf{1}^+$ (herein summarized as $[Cu^I(HL^N_{IBQ})_2]^+$), showing the metal and ligand oxidation states.

The CV of complex **2** exhibits two anodic peaks at E_p^{a1} = –0.37 and E_p^{a2} = –0.13 V vs. Fc^+/Fc (Figure 2b), the first being associated to twin cathodic peaks at E_p^{c1} = –0.39 and $E_p^{c1'}$ = –0.44 V. These redox waves are assigned to ligand-centered processes. Two irreversible oxidation waves are additionally detected at E_p^{a3} = 0.78 and E_p^{a4} = 0.97 V.

The stability of the anion $\mathbf{1}^-$, neutral **1** and dication $\mathbf{1}^{2+}$, as well as the nature of the first oxidation waves of **2** were investigated by bulk electrolysis at 298 K under Ar.

Both **1** and $\mathbf{1}^{2+}$ are stable on the time scale of electrolysis, as verified by the similarities between their CV curves and that of starting $\mathbf{1}^+$. A slight but significant difference is observed between the CV of $\mathbf{1}^{2+}$ and that of $\mathbf{1}^+$, whereby E_p^{c1} (Cu^{II}/Cu^I redox couple) is observed at –0.25 V instead of –0.15 V on the first scan (see ESI). This reflects an increased stability of the dication, presumably by more favorable solvation and/or a reorganization of the coordination sphere during electrolysis.

The two-electron reduction of $\mathbf{1}^+$ produces significant changes in the CV (see ESI), suggesting that the anion $\mathbf{1}^-$ evolves during experiment. It is significant that the so-obtained CV shows the distinct features of **2**. Hence the anion $\mathbf{1}^-$ likely evolves towards **2** during electrolysis. This conversion is also supported by spectro-electrochemical measurements (see below). Given the absence of dioxygen (glove box) we ruled out an air-promoted rearrangement of the complex. A possible mechanism would thus involve the initial formation of $\mathbf{1}^-$, which evolves by releasing one $(HL^N_{ISQ})^-$ ligand molecule. This latter molecule may then act as an oxidant towards the (1:1) complex to give **2**. Related disproportionation reactions were documented for some complexes of H_3L^O.[3f]

Strikingly, the electrochemical oxidation of **2** at 0.4 V results in the growing of the waves reminiscent of $\mathbf{1}^+$ in the CV curve (Figure 2b, red line). Hence the trimer is dissociated upon oxidation. Most probably oxidation of the ligand decreases its charge and subsequent coordinating ability making it unable to stabilize oligomeric structures.

DFT Calculations

The electronic structures of $\mathbf{1}^+$, **2** and the corresponding accessible oxidation states have been investigated by DFT calculations, at the TPSSh level of theory.

For the cation $\mathbf{1}^+$ we considered three putative electronic structures: A closed-shell singlet that corresponds to a Cu(I) metal ion coordinated to two HL_N^{IBQ} ligands, a triplet resulting from a Cu(II) center ferromagnetically exchange coupled to one $(HL_N^{ISQ})^-$ ligand (the other adopting the HL_N^{IBQ} form), as well as the associated broken symmetry singlet. The closed-shell singlet is greatly favored, as it lies 11.5 kcal/mol below the triplet, and also below the broken symmetry singlet. This clearly shows that $\mathbf{1}^+$ is a genuine Cu(I) complex. It is worth noting that the large tetrahedral distortion at the metal center, which manifests by a τ_4 index of 0.43 in the optimized structure of the singlet, compares fairly well with the experimental value.

For the dication $\mathbf{1}^{2+}$ we considered only a doublet state, in agreement with EPR data (see below). In the optimized structure of $\mathbf{1}^{2+}$ the metal ion is pentacoordinate and adopts a geometric intermediate between square pyramidal and trigonal bipyramid (Figure 3). This result corroborates the electrochemical data which points to a significant rearrangement upon oxidation of $\mathbf{1}^+$ to $\mathbf{1}^{2+}$. The Mulliken spin population in $\mathbf{1}^{2+}$ is mainly located at the metal (0.65), with smaller spin population onto the chelating nitrogen atoms due to the covalency of the coordination bonds. This demonstrates that $\mathbf{1}^{2+}$ has a Cu(II) bis(HL_N^{IBQ}) character (Scheme 2).

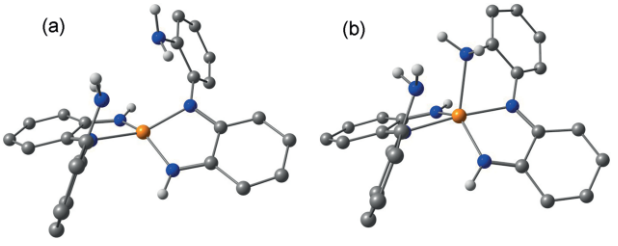

Figure 3. Optimized structures of (a) $\mathbf{1}^+$ and (b) $\mathbf{1}^{2+}$, with selected bond lengths. Selected H as well as the *tert*-butyl groups are omitted for clarity.

The neutral complex **1** can be described as either a $[Cu^I(HL_N^{ISQ})(HL_N^{IBQ})]$ complex (doublet spin state) or a diradical $[Cu^{II}(HL_N^{ISQ})_2]$ species (quartet or broken symmetry doublet spin state). The energetic analysis points to a doublet ground spin state, with a doublet-quartet gap of 9.3 kcal/mol. Notably the $\langle S \rangle^2$ in the doublet is 0.85, with a slightly negative spin population at the copper center (–0.16) and a positive spin population at the coordinating nitrogen atoms (+0.13 and +0.17). The spin contamination, as well as this small spin density at the copper point to a small energy gap between the genuine doublet $[Cu^I(HL_N^{ISQ})(HL_N^{IBQ})]$ and the broken symmetry singlet $[Cu^{II}(HL_N^{ISQ})_2]$, the first being the ground spin state.

The hypothetical $\mathbf{1}^-$ complex was also computed. Both the triplet and singlet spin states were calculated, and the energy gap was found to be 2.8 kcal/mol. Due to this small value it is not possible to unambiguously assign the ground spin state of the anion on the sole basis of an energetic analysis. Since $\mathbf{1}^-$ evolves once generated (see above) we did not investigate further its detailed electronic structure.

The electronic structure of **2** was first regarded by using a frozen structure (coming from X-ray crystallography) because of the prohibitive computational cost for DFT calculations on such cluster. Single point energy calculations were first undertaken

on the heptet, closed-shell singlet and open-shell singlet. They demonstrate that the singlet lies 17 kcal/mol below the heptet, but its wavefunction shows an UHF/RHF instability. Hence the open-shell singlet, which corresponds to a broken symmetry state is the lowest energy state. We secondly optimized the heptet and computed the associated broken-symmetry state. Despite that mono-determinant DFT is not the most appropriate method to investigate such complicated systems, some meaningful information can be extracted from calculations. Positive spin population is indeed found at each copper center and negative spin population is predicted on the coordinating nitrogen atoms of the three ligands in the open-shell doublet. This suggests antiferromagnetic interactions between each radical ligand $(L^{N}_{ISQ})^{2-}$ and the coordinated copper centers, which all adopt a (+II) oxidation state in **2**.

EPR Spectroscopy

The starting complexes $\mathbf{1}^{+}$ and **2** are EPR silent in CH_2Cl_2 due to their diamagnetic ground spin states. Conversely, **1** and $\mathbf{1}^{2+}$ show (S = 1/2) resonances (Figure 4), which provide important information regarding their electronic structure. Each complex exhibits a four line pattern that can be interpreted by the hyperfine interaction of the electronic spin with the copper nucleus (I_{Cu} = 3/2). The following spin Hamiltonian parameters were determined for complex **1**: g_{iso} = 1.998, $|A_1|$ = $|A_2|$ = 22 MHz, $|A_3|$ = 73 MHz for a single copper nucleus. The fact that the g value is isotropic and close to the free electron value (g_e = 2.0023) demonstrates a predominant radical character of the complex. Furthermore, the hyperfine coupling constants are much lower than those classically observed for Cu(II) ions.[2,3c] In other terms this spectrum can be interpreted by the coordination of a ligand radical to a diamagnetic Cu(I) center. In order to confirm this interpretation, we computed the spin Hamiltonian parameters by DFT. We obtained a reasonable agreement with experiment, as the computed parameters are g_x = 2.000, g_y = 1.997, g_z = 1.965 (g_{iso} = 1.988) and A_{Cux} = –92 MHz, A_{Cuy} = –52 MHz and A_{Cuz} = 126 MHz.

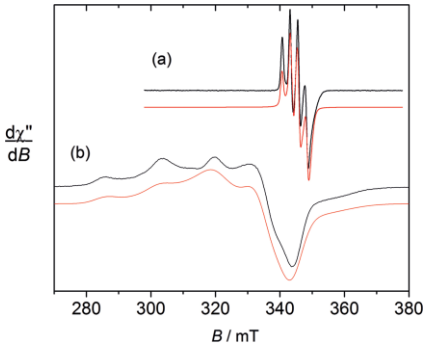

Figure 4. EPR spectra of (a) **1**, (b) $\mathbf{1}^{2+}$ in 0.5 mM CH_2Cl_2 solution containing 0.1 M TBAP. Microwave Freq. 9.636 GHz; power, 5 mW. Mod. Freq. 100 kHz; Amp. 0.4 mT. T = 18 K. Black lines are experimental spectra, red lines are simulations using the parameters given in the text.

The spectrum of the dication $\mathbf{1}^{2+}$ was simulated by considering both an unresolved copper signal and an isolated mononuclear copper complex, the latter exhibiting the following spin Hamiltonian parameters: $g_x = g_y$ = 2.050, g_z = 2.214, with $A_x = A_x$ = 20 MHz, A_z = 517 MHz. The higher g-tensors, the significant anisotropy and the larger A_{Cu} point to a metal centered magnetic orbital. Hence the dication features a Cu(II) center coordinated to two closed-shell ligands. The spin Hamiltonian parameters were again computed by DFT, giving g_x = 2.015, g_y = 2.065, g_z = 2.100 (g_{iso} = 2.060) while the A_{Cu} are A_x = 199 MHz, A_y = –135 MHz and A_z = –414 MHz. As previously documented for copper complexes the computed g_{iso} is smaller than the experimental value due to the tendency of DFT to overestimate the covalency of the coordination bonds.[12] Apart from this expected behavior, the trend of g and A between **1** and $\mathbf{1}^{2+}$ is correctly predicted by DFT, further validating our theoretical approach.

UV/Vis-NIR Spectroscopy and TD-DFT Calculations

Complexes $\mathbf{1}^{+}$ and **2** are deeply colored and show intense absorptions over both the visible and NIR regions (Figure 5, Figure 6, Table 3). Complex $\mathbf{1}^{+}$ exhibits a remarkable NIR band at 980 nm (22 080 M^{-1} cm^{-1}), that is assigned by TD-DFT to HOMO → LUMO and corresponds mainly to a ligand-to-ligand charge transfer transition from a delocalized ligand orbital to the iminobenzoquinone cores (λ_{calcd} = 796 nm, f_{osc} = 0.349). Upon oxid-

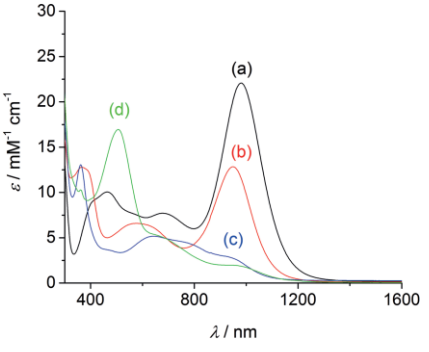

Figure 5. UV/Vis-NIR spectra of (a, black) $\mathbf{1}^{+}$, (b, red) **1**, (c, blue) "two-electron reduced" $\mathbf{1}^{-}$, (d, green) $\mathbf{1}^{2+}$ in 0.5 mM CH_2Cl_2 solution containing 0.1 M TBAP (except d, which was generated by adding one molar equiv. of $AgSbF_6$). For the two-electron reduction the molar extinction coefficient is based on the total copper concentration.

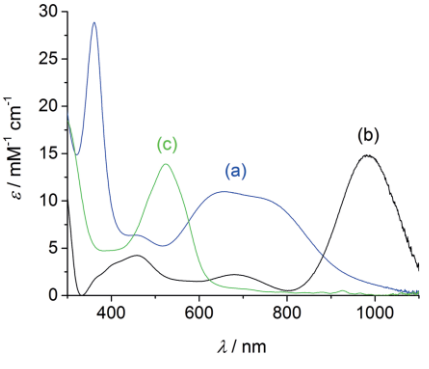

Figure 6. UV/Vis-NIR spectra of **2**. (a, blue) before electrolysis, (b, black) after exhaustive electrolysis at +0.2 V, (c, green) exhaustive electrolysis at +0.4 V in 0.5 mM CH_2Cl_2 solution containing 0.1 M TBAP.

Full Paper
doi.org/10.1002/ejic.202000379

ation to $\mathbf{1}^{2+}$ this intense band vanishes, replaced by a broad unresolved NIR feature of lower intensity with shoulders at ca. 640 and 960 nm, as well as a predominant band at 505 nm (16 960 M^{-1} cm^{-1}). Consistently, TD-DFT calculations do not predict electronic excitations with oscillator force greater than 0.05 above 560 nm. The most intense excitation is predicted at 552 nm (f_{osc} = 0.1239), and accounts for the experimental band at 551 nm. Several electronic excitations contribute to this excitation, which is principally due to an intraligand CT within the tris-ligated ligand. Reduction into neutral **1** is accompanied by a shift of the NIR band towards 948 nm, whose intensity decreased by one half (12 840 M^{-1} cm^{-1}). It is assigned to β-HOMO → β-LUMO and corresponds mainly to CT from the whole ligands to the iminobenzoquinone or iminosemiquinone cores (λ_{calcd} = 914 nm, f_{osc} = 0.211). Further reduction of **1** results in a severe broadening of the Vis-NIR features, which expand from 500 to 1000 nm with intensity lower than 5500 M^{-1} cm^{-1}. The main peak is at 645 nm (5170 M^{-1} cm^{-1}), with shoulders at 770 and 930 nm. By TD-DFT we recalculated the spectrum of the anion $\mathbf{1}^{-}$. An intense NIR band is predicted for the singlet (λ_{calcd} = 1017 nm, f_{osc} = 0.178), which contrasts sharply with experiment. We take this as further evidence for the rearrangement of the monoanion into **2** (see above).

Table 3. UV/Vis-NIR properties of the complexes.[a]

Complex	λ [nm] (ε [mM^{-1} cm^{-1}])
1red[b]	362 (13 060), 645 (5170), 770sh (4460), 930sh (2900)
1	366 (12 790), 578 (6590), 948 (12 840)
$\mathbf{1}^{+}$	464 (10 052), 676 (7710), 980 (22 080)
$\mathbf{1}^{2+}$	505 (16 960), 640sh (5400), 960sh (1950)
2	361 (28 860), 653 (10 980), 770sh (9790)
2ox[c]	460 (4241), 679 (2210), 980 (14 860)
2ox′[c]	523 (13 890), 650 sh (700)

[a] In CH_2Cl_2 containing 0.1 M TBAP. [b] After exhaustive electrolysis of $\mathbf{1}^{+}$ at −1.6 V. [c] After exhaustive electrolysis of **2** at +0.2 V (**2ox**) or +0.4 V (**2ox′**).

The spectrum of **2** consists of a band at 653 nm (10 980 M^{-1} cm^{-1}), with a shoulder at 770 nm (Figure 6a). DFT calculations predict several low energy excitations (f_{osc} < 0.05), which account for the NIR tail. Its single oxidation produces a chromophore that absorbs strongly at 980 nm (14 860 M^{-1} cm^{-1}, Figure 6b), similarly to $\mathbf{1}^{+}$, while double oxidation affords a species that shows a dominant band at 523 nm (13 890 M^{-1} cm^{-1}, Figure 6c) associated to a low intensity NIR tail and hence compares with $\mathbf{1}^{2+}$. These spectroscopic data are thus consistent with electrochemistry, demonstrating that oxidation of the trimer **2** produces a mononuclear complex, either $\mathbf{1}^{+}$ or $\mathbf{1}^{2+}$, depending on the applied potential.

Electrocatalytic Reduction of Dioxygen and Hydrogen Peroxide

Tricopper centers are found in laccases,[13] which catalyze the four electron reduction of dioxygen into water. This has prompted us to investigate the electrocatalytic properties of **2** towards dioxygen and its two-electron reduced form, hydrogen peroxide. We exploited the presence of multiple hydrophobic *tert*-butyl groups and aromatic rings to adsorb complex **2** onto multiwall carbon nanotubes (MWCNT). Complex **2** does not catalyze dioxygen reduction but exhibits electrocatalytic activity regarding reversible hydrogen peroxide reduction. The CV for MWCNT functionalized by complex **2** both under argon and in the presence of 10 mM H_2O_2 is depicted in Figure 7. For comparison the CV of MWCNT electrodes functionalized with horseradish peroxidase (HRP), a well-known H_2O_2-reducing metalloenzyme is also included. This enzyme was immobilized by boronic-ester covalent binding with a pyrene-boronic-acid linker, as previously reported.[14]

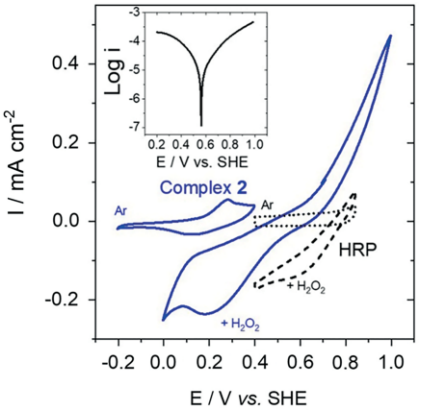

Figure 7. Cyclic voltammetry for (blue straight line) complex **2**-functionalized MWCNT electrodes (acetate buffer, pH 5) and HRP-functionalized MWCNT electrodes (phosphate buffer, pH 7) under Ar before and after addition of 10 mM H_2O_2 (v = 10 mV s^{-1}, ref. SHE); (inset) Tafel plot for complex **2**-functionalized MWCNT electrodes (acetate buffer, pH 5).

First, CV under argon confirms the stable adsorption of the complex **2** in water. This is indicated by the presence of a poorly-reversible redox system, which is preserved after several repeated CV scans and corresponds to the oxidation of immobilized complex **2**. This stable adsorption might be favored by the strong hydrophobic pi–pi interaction brought about by the three polycyclic ligands with CNT sidewalls. A surface coverage of Γ_{max} = 76 pmol cm^{-2} for complex **2** was estimated by integration of the charge of the anodic peak under argon. After addition of 10 mM H_2O_2, the **2**-functionalized MWCNTs exhibit electrocatalytic activity towards both H_2O_2 reduction and oxidation. It is noteworthy that pristine MWCNT electrodes do not show any electrocatalytic activity towards H_2O_2 in the same potential window. Tafel analysis indicates an onset potential of E_{onset} = +0.56 V vs. SHE. Maximum current density of 0.22 mA cm^{-2} was measured with an apparent turnover frequency (TOF) of 15 s^{-1} by taking into account the surface coverage by complex **2**. A plausible electrocatalytic mechanism might involve the oxidation of complex **2** by H_2O_2, generating the catalytically active species. It is noteworthy that the Tafel slopes were measured at 130 mV per decade, indicative of a rate-determining one-electron. However, exhaustive studies will be required in order to identify if copper-peroxo intermediate are involved, as well as potential ligand exchange in complex **2**. For comparison, HRP is able to reduce H_2O_2 at higher onset potentials of E_{onset} = +0.83 V vs. SHE (pH 7) at modified MWCNT electrodes.[14,15] A deca-heme cytochrome exhibits onset potential of +0.72 V (pH 6.5) on a porous ITO electrode,[16] while bioinspired iron-por-

phyrin complexes exhibits onset potentials of 0.7 V at pH 7.[15,17] It must be stressed that we recently immobilized mono and dicopper-phenolato complexes which exhibit smaller onset potentials of + 0.33 V (pH 4) towards both O_2 and H_2O_2 reduction.[11c,18] Thus, despite the fact that only 150 mV are still to be gained in order to reach the best iron-porphyrin-based catalyst efficiency, these tricopper complexes represent a novel family of promising molecular electrocatalysts based on earth abundant metals for H_2O_2 reduction under mild conditions.

Conclusion

In summary, we demonstrate that the pincer ligand H_3L^N can stabilize copper in both its +I and +II oxidation states. Depending on the copper source used for the synthesis and the potential applied during electrolysis two complexes with distinct stoichiometries form: A mononuclear (1:2) or trinuclear (3:3) complex. None of the structures herein reported were observed for the copper complexes of the related pincer ligand H_3L^O (Scheme 4).[3f,j,s]

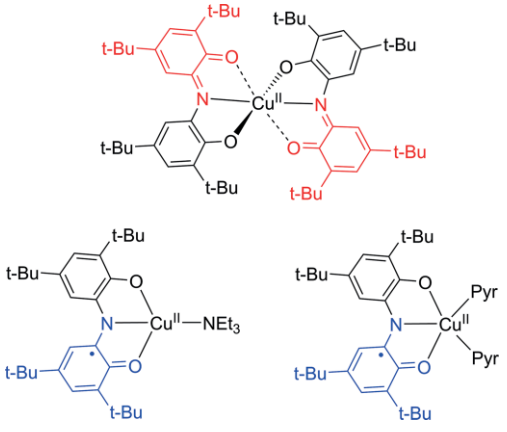

Scheme 4. Structure of -crystallized copper complexes of H_3L^{O}[3f,j] containing one fully oxidized arm (benzoquinone, shown in red) or one iminosemiquinone radical arm (blue).

We establish that the distinct basicity of the peripheral donors of H_3L^N allowed for a bis(bidentate) ligation, with one amine of each ligand remaining in its NH_2 form. The NH_2 groups adopt a *cis*-configuration and each is involved in H-bonding interactions with a SbF_6^- molecule. The steric clash induced by the bulky ligands enforce strong tetrahedral distortions favorable to monovalent copper. In the H_3L^O chelate the terminal carbonyl groups are coordinating, giving an octahedral geometry with Jahn–Teller distortion that is suitable for Cu(II).[3f] Notably the carbonyl groups bind in *trans* configuration, at each apical position. Another striking difference is the oxidation state of the loosely bound (or unbound) unit: In the case of H_3L^O, it is the fully oxidized (quinone) unit, which is a poor donor, whereas in $\mathbf{1}^+$ it is unoxidized diaminobenzene unit.

Complex **2** is trinuclear, which is an unprecedented stoichiometry for this family of pincer ligands (N3 or N2O chelates). The fourth coordination in the fully deprotonated (1:1) complex is occupied by the anilido nitrogen of a neighboring ligand, despite the excess of Et_3N used for the synthesis.

We did not isolate a monomer with one bound triethylamine, as reported by Wieghardt for the H_3L^O counterpart,[3j] which may be another consequence of the distinct basicity of the peripheral donors.

Another striking point is the peculiar redox properties the H_3L^N complexes: First the potentials are in general much lower than for the copper complexes of H_3L^O, allowing for the isolation of a cationic and not a neutral monomeric species. Secondly, the oxidation potentials in the H_3L^O chelates are > +0.13 V and correspond to ligand-centered processes,[3b,c,j] whereas the first oxidation is observed as low as –0.37 for $\mathbf{1}^+$ and corresponds to a metal-centered process. Furthermore, we evidenced an unprecedented redox interconversion for H_3L^N, whereby the monomeric species can be converted upon reduction into the trimer **2** and vice versa.

Finally, owing to a stable immobilization at nanostructured electrodes, complex **2** exhibits electrocatalytic activity towards reversible H_2O_2 reduction at high potentials of 0.53 V. This work demonstrates the first example of an electrode functionalized with a tricopper complex active towards high potential H_2O_2 reduction in mild aqueous conditions. Further studies are in progress in order to decipher the electrocatalytic mechanism as well as study their use in peroxidase-like sensors or in H_2O_2-based fuel cells where high potentials are required towards H_2O_2 reduction.

Experimental Section

General

Unless otherwise noted, all operations were performed under anaerobic conditions under a pure argon atmosphere using standard Schlenk techniques. Anhydrous triethylamine was distilled from CaH_2 under an argon atmosphere prior to use. Anhydrous acetonitrile and methanol were purchased from Acros. NMR spectra were recorded on a Bruker Avance 400 (^{1}H at 400 MHz, ^{13}C at 100 MHz). Chemical shifts are given relative to solvent residual peaks. Mass spectra were recorded on a Bruker Esquire 3000 (ESI/Ion Trap) equipment. Microanalysis were performed by using an apparatus designed by the Service Central d'Analyse du CNRS (Lyon, France). UV/Vis spectra were recorded on a Perkin-Elmer Lambda 1050 spectrophotometer in quartz cells (Hellma) of 1.00 mm path length. X-band EPR spectra were recorded on an EMX plus spectrometer equipped with an Oxford Helium cryostat. Spectra were simulated using the Easyspin software package.[19] Electrochemical measurements were carried out using a BioLogic SP300 potentiostat or a CH Instruments 620 potentiostat. Experiments were performed in a standard three-electrode cell under argon atmosphere in CH_2Cl_2 solutions containing 0.1 M tetrabutylammonium perchlorate (TBAP) as supporting electrolyte. An $Ag/AgNO_3$ (0.01 M) reference electrode was used. All the potentials given in the text are referred to the regular Fc^+/Fc redox couple used as an internal reference. A glassy carbon disc electrode (5 mm diameter), which was polished with 1 mm diamond paste, was used as the working electrode. RDE experiments were performed by using a Radiometer CTV101 unit. Electrolyses were conducted at constant applied potential by using a carbon plate as working electrode.

Electrocatalysis

Commercial grade thin multi-walled carbon nanotubes (MWCNT, 9.5 nm diameter, purity >95 %) were obtained from Nanocyl and

used as received without any purification step. The electrochemical experiments in aqueous media were performed in 0.1 M acetate buffer pH 5 or 0.1 M phosphate buffer pH 7 in a three-electrode electrochemical cell using an Autolab pgstat100 potentiostat. The surface of GC electrodes was polished with a 2 μm diamond paste purchased from Presi (France) and rinsed successively with water, acetone, and ethanol. A Pt wire placed in a separated compartment was used as counter electrode, and the Ag/AgCl (KCl sat) served as a reference electrode. Horseradish peroxidase/MWCNT electrode was prepared according to a previously-described procedure.[15] GC electrode was drop-casted with 20 uL of MWCNT suspension (5 mg/mL in NMP). A homogeneous CNT film was obtained after drying under vacuum for 1 hour, affording a 0.2 cm^2 MWCNT electrode. MWCNT electrodes were soaked in a solution of 3 mM of complex **2** for 1 hour, then rinsed with DMF and dried. Electrochemical characterizations were carried in a 0.1 M acetate buffer pH 5 under argon to prevent any contribution of dissolved oxygen on the recorded measures. 10 mM of H_2O_2 was then added to the electrolyte to assess the catalytic activity of the immobilized copper complex.

Crystal structure analysis

A single crystal was coated with a parafin mixture, picked up with nylon loops and mounted in the nitrogen cold stream of a Nonius 4 circles diffractometer at 200 K. The Mo-K_α radiation (λ = 0.71073Å) from an Incoatec micro Mo-target X-ray source equipped with Montel optics was used. The data were collected with a Bruker APEXII detector. Final cell parameters were obtained from refinements using the whole data. Intensities were integrated and corrected for Lorentz and polarization factor using EVAL14 then corrected for absorption using a multiscan method implemented with the program SADABS and then finally merged using XPREP. The structures were solved and refined by charge flipping methods and subsequent difference Fourier techniques. The OLEX software was used for the refinement.[20] All non-hydrogen atoms were anisotropically refined and hydrogen atoms were placed at calculated positions and refined as riding atoms with isotropic displacement parameters. Both compounds crystallized as twins. For **1**$^+$(SbF_6^-) the two lattices could have been identified and integrated separately with a rate of 60.15 % vs. 39.85 %. The numerous overlaps in the data prevented the obtaining of a really accurate structure. For compound **2** we simply used the following twin law:

$$\begin{pmatrix} 1 & 0 & 0 \\ 0 & 1 & 0 \\ 0 & 0 & -1 \end{pmatrix}$$

The rate between the two lattices is of 63.48 % vs. 36.16 %.

Deposition Number 1989039 and 1989040 contain the supplementary crystallographic data for this paper. These data are provided free of charge by the joint Cambridge Crystallographic Data Centre and Fachinformationszentrum Karlsruhe Access Structures service http://www.ccdc.cam.ac.uk/structures.

Computational details

Full geometric optimizations were performed with the Gaussian 9.0 program.[21] The TPSSh functional[22] was used together with the 6-31g* basis set for the C,H,N atoms.[23] Frequency calculations were systematically performed in order to ensure that the optimized structures correspond to a real energy minimum and not a saddle point. The relative energies were obtained from single-point calculations and corrected from the ZPE using the same level of theory (functional and basis sets). Electronic transition energies for all complexes were calculated using time-dependent DFT (TD-DFT).[24] The solvent effect was considered by using a polarizable continuum model[25] and the 40 lowest energy excited states were calculated.

Synthesis

The synthetic procedure for the preparation of H_3L^N was reported elsewhere.[6a]

[Cu(HL$^N_{IBQ}$)$_2$](SbF_6). $CuCl_2$ (16 mg, 0.12 mmol, 0.5 equiv.) and Et_3N (66 μL, 0.47 mmol, 2.0 equiv.) were added to a solution of H_3L^N (100 mg, 0.24 mmol, 1.0 equiv.) in MeOH (12 mL). The mixture was immediately heated to 80 °C and rapidly turned black. After 15 min, $KSbF_6$ (199 mg, 0.72 mmol, 3.0 equiv.) was added and the mixture was refluxed during 45 min. While cooling the reaction to r.t., a black precipitate formed. The suspension was cooled to 5 °C with an ice bath and the precipitate was filtered through a frit and washed with cold MeOH. Yield: 68 %; ^{1}H NMR (400 MHz, CD_2Cl_2): δ (ppm)= 7.83 (br s, 2H, N*H*), 7.38 (s, 2H, H_{Ar}), 7.15 (s, 2H, H_{Ar}), 6.96 (d, J = 2.4 Hz, 2H, H_{Ar}), 6.88 (br s, 2H, H_{Ar}), 4.67 (br s, 4H, N*H*), 1.42 (s, 18H, *t*-Bu), 1.34 (s, 18H, *t*-Bu), 1.17 (s, 18H, *t*-Bu), 1.12 (br s, 18H, *t*-Bu); ^{13}C NMR (100 MHz, CD_2Cl_2): δ (ppm)= 162.3, 155.7, 144.2, 140.5, 140.4, 137.2, 135.6, 128.4, 125.4, 118.2, 115.1, 36.8, 35.30, 35.27, 34.9, 31.9, 30.8, 30.1, 29.2. MS (ESI): *m/z*= 606 [M – SbF6]$^+$. IR: ν (cm^{-1}) 3528, 3417, 3379, 2955, 2908, 2867, 1610, 1477, 1461, 1277, 1261, 761, 748. Anal. Calcd for $C_{56}H_{86}N_6CuSbF_6$: C, 58.85; H, 7.60; N, 7.36; found C, 59.13; H, 7.71; N, 7.67.

[Cu$_3$(L$^N_{ISQ}$)$_3$]·CH_3CN. Under argon, to a degassed solution of $Cu(CH_3CN)_4{\cdot}PF_6$ (880 mg, 2.36 mmol, 1.0 equiv.) in MeCN (12 mL) were added the ligand H_3L^N (1.0 g, 2.36 mmol, 1.0 equiv.) and triethylamine (2.3 mL, 16.50 mmol, 7.0 equiv.). The mixture was refluxed for 1 hour and subsequently exposed to air while cooling to r.t. After an additional hour whilst stirring at r.t., the mixture was cooled with an ice bath. The black precipitate that formed was filtered through a frit, abundantly washed with cold MeCN and dried under vacuum to afford a greenish black microcrystalline powder (1.01 g, 0.68 mmol, yield= 86 %). An analytically pure sample was obtained from a CH_2Cl_2 solution layered with CH_3CN. Single crystals suitable for X-ray analysis were obtained by vapor diffusion at r.t. of MeCN into a benzene solution of the complex. ^{1}H NMR (400 MHz, CD_2Cl_2): δ (ppm)= 8.28 (s, 3H, H_{Ar}), 7.74 (s, 3H, H_{Ar}), 7.46 (s, 3H, H_{Ar}), 7.22 (s, 3H, H_{Ar}), 5.77 (br s, 3H, N*H*), 2.16 (br s, 3H, N*H*), 1.97 (s, 3H, CH_3CN), 1.71 (s, 27H, *t*-Bu), 1.40 (s, 27H, *t*-Bu), 1.21 (s, 27H, *t*-Bu), 0.95 (s, 27H, *t*-Bu). ^{13}C NMR (100 MHz, CD_2Cl_2): δ (ppm)= 155.9, 146.0, 145.0, 144.0, 143.7, 143.2, 142.4, 140.7, 119.2, 116.6, 114.9, 114.2, 36.9, 35.8, 35.4, 35.2, 32.4, 31.8, 31.3, 29.9. MS (ESI): *m/z*= 551 [M + H]$^+$. IR: ν (cm^{-1}) 3361, 3317, 2954, 2899, 2867, 1457, 1362, 1151. Anal. Calcd for $C_{84}H_{126}Cu_3N_9$, CH_3CN, 0.5 CH_2Cl_2: C, 67.53; H, 8.53; N, 9.12; found C, 67.54; H, 8.64; N, 8.92.

Acknowledgments

The authors thank the Labex ARCANE (CBH-EUR-GS/ANR-17-EURE-0003) for financial support. This work was supported by the Ministère de l'Environnement, de l'Energie et de la Mer and the Agence Nationale de la Recherche through the LabEx ARCANE programe (ANR-11-LABX-0003-01). The authors are grateful to Dr. Pierre Girard for technical assistance for the DFT calculations and the Centre de Calcul Intensif en Chimie de Grenoble (CECIC) for providing the computational resources. The Nano-

bio-ICMG Platform (FR 2607) is acknowledged for analytical support.

Keywords: Copper · Phenylenediamine · Radicals · Electronic structure · Iminosemiquinones

[1] a) P. J. Chirik, K. Wieghardt, *Science* **2010**, *327*, 794–795; b) O. R. Luca, R. H. Crabtree, *Chem. Soc. Rev.* **2013**, *42*, 1440–1459; c) F. Novio, E. Evangelio, N. Vazquez-Mera, P. González-Monje, E. Bellido, S. Mendes, N. Kehagias, D. Ruiz-Molina, *Sci. Rep.* **2013**, *3*, 1708; d) D. L. J. Broere, R. Plessius, J. I. van der Vlugt, *Chem. Soc. Rev.* **2015**, *44*, 6886–6915; e) S. Demir, I.-R. Jeon, J. R. Long, T. D. Harris, *Coord. Chem. Rev.* **2015**, *289–290*, 149–176; f) B. de Bruin, P. Gualco, N. D. Paul in *Redox Non-innocent Ligands*, (Ed.: M. S. a. R. J. Lundgren), **2016**, pp. 176–204; g) I.-R. Jeon, L. Sun, B. Negru, R. P. Van Duyne, M. Dincă, T. D. Harris, *J. Am. Chem. Soc.* **2016**, *138*, 6583–6590; h) J. A. DeGayner, K. Wang, T. D. Harris, *J. Am. Chem. Soc.* **2018**, *140*, 6550–6553.

[2] A. Y. Girgis, A. L. Balch, *Inorg. Chem.* **1975**, *14*, 2724–2727.

[3] a) S. K. Larsen, C. G. Pierpont, *J. Am. Chem. Soc.* **1988**, *110*, 1827–1832; b) C. L. Simpson, S. R. Boone, C. G. Pierpont, *Inorg. Chem.* **1989**, *28*, 4379–4385; c) B. G. Maiya, Y. Deng, K. M. Kadish, *J. Chem. Soc., Dalton Trans.* **1990**, 3571–3576; d) C. G. Pierpont, C. W. Lange in *The Chemistry of Transition Metal Complexes Containing Catechol and Semiquinone Ligands*, **1994**, pp. 331–442; e) S. N. Lyubchenko, V. A. Kogan, L. P. Olekhnovich, *Russ. J. Coord. Chem.* **1996**, *22*, 534–540; f) G. Speier, J. Csihony, A. M. Whalen, C. G. Pierpont, *Inorg. Chem.* **1996**, *35*, 3519–3524; g) M. A. Brown, J. A. Castro, B. R. McGarvey, D. G. Tuck, *Can. J. Chem.* **1999**, *77*, 502–510; h) C. Camacho-Camacho, G. Merino, F. J. Martínez-Martínez, H. Nöth, R. Contreras, *Eur. J. Inorg. Chem.* **1999**, *1999*, 1021–1027; i) P. Chaudhuri, M. Hess, K. Hildenbrand, E. Bill, T. Weyhermüller, K. Wieghardt, *Inorg. Chem.* **1999**, *38*, 2781–2790; j) P. Chaudhuri, M. Hess, T. Weyhermüller, K. Wieghardt, *Angew. Chem. Int. Ed.* **1999**, *38*, 1095–1098; *Angew. Chem.* **1999**, *111*, 1165; k) N. G. Furmanova, S. N. Lyubchenko, V. Kogan, L. P. Olekhnovich, *Cryst. Rep.* **2000**, *45*, 439–443; l) D. Ruiz-Molina, J. Veciana, K. Wurst, D. N. Hendrickson, C. Rovira, *Inorg. Chem.* **2000**, *39*, 617–619; m) A. Piskunov, I. Smolyaninov, O. Yu. Sukhoshkina, *Russ. J. Gen. Chem.* **2010**, *80*, 790–799; n) A. V. Piskunov, O. Y. Trofimova, S. Y. Ketkov, G. K. Fukin, V. K. Cherkasov, G. A. Abakumov, *Russ. Chem. Bull.* **2011**, *60*, 2522–2530; o) G. Szigethy, A. F. Heyduk, *Dalton Trans.* **2012**, *41*, 8144–8152; p) G. Szigethy, D. W. Shaffer, A. F. Heyduk, *Inorg. Chem.* **2012**, *51*, 12606–12618; q) J. L. Wong, R. H. Sánchez, J. G. Logan, R. A. Zarkesh, J. W. Ziller, A. F. Heyduk, *Chem. Sci.* **2013**, *4*, 1906–1910; r) A. A. Maleev, O. Y. Trofimova, A. P. Pushkarev, N. V. Somov, V. V. Travkin, G. L. Pakhomov, A. V. Piskunov, M. N. Bochkarev, *Nanotechnol. Russ.* **2015**, *10*, 613–620; s) J. Jacquet, K. Cheaib, Y. Ren, H. Vezin, M. Orio, S. Blanchard, L. Fensterbank, M. Desage-El Murr, *Chem. Eur. J.* **2017**, *23*, 15030–15034.

[4] a) N. Ito, S. E. V. Phillips, C. Stevens, Z. B. Ogel, M. J. McPherson, J. N. Keen, K. D. S. Yadav, P. F. Knowles, *Nature* **1991**, *350*, 87–90; b) B. P. Branchaud, B. E. Turner in *30 - Galactose Oxidase: Probing Radical Mechanism with Ultrafast Radical Probe, Vol. 354* (Ed.: D. L. Purich), Academic Press, **2002**, pp. 415–425; c) J. W. Whittaker, *Chem. Rev.* **2003**, *103*, 2347–2364; d) D. Rokhsana, D. M. Dooley, R. K. Szilagyi, *J. Am. Chem. Soc.* **2006**, *128*, 15550–15551; e) F. Thomas, *Eur. J. Inorg. Chem.* **2007**, *2007*, 2379–2404; f) D. Yin, S. Urresti, M. Lafond, E. M. Johnston, F. Derikvand, L. Ciano, J.-G. Berrin, B. Henrissat, P. H. Walton, G. J. Davies, H. Brumer, *Nat. Commun.* **2015**, *6*, 10197; g) A. K. Chaplin, C. Bernini, A. Sinicropi, R. Basosi, J. A. R. Worrall, D. A. Svistunenko, *Angew. Chem. Int. Ed.* **2017**, *56*, 6502–6506; *Angew. Chem.* **2017**, *129*, 6602.

[5] a) P. Chaudhuri, M. Hess, U. Flörke, K. Wieghardt, *Angew. Chem. Int. Ed.* **1998**, *37*, 2217–2220; *Angew. Chem.* **1998**, *110*, 2340; b) T. K. Paine, T. Weyhermüller, K. Wieghardt, P. Chaudhuri, *Dalton Trans.* **2004**, 2092–2101.

[6] a) N. Leconte, J. Moutet, K. Herasymchuk, R. M. Clarke, C. Philouze, D. Luneau, T. Storr, F. Thomas, *Chem. Commun.* **2017**, *53*, 2764–2767; b) N. Leconte, J. Moutet, T. Constantin, F. Molton, C. Philouze, F. Thomas, *Eur. J. Inorg. Chem.* **2018**, *2018*, 1752–1761.

[7] N. Leconte, B. Baptiste, C. Philouze, F. Thomas, *Dalton Trans.* **2018**, *47*, 11303–11307.

[8] L. Yang, D. R. Powell, R. Houser, *Dalton Trans.* **2007**, 955–964.

[9] S. Ye, B. Sarkar, F. Lissner, T. Schleid, J. van Slageren, J. Fiedler, W. Kaim, *Angew. Chem. Int. Ed.* **2005**, *44*, 2103–2106; *Angew. Chem.* **2005**, *117*, 2140.

[10] a) H.-Y. Cheng, C.-C. Lin, B.-C. Tzeng, S.-M. Peng, *J. Chin. Chem. Soc.* **1994**, *41*, 775–781; b) D. Herebian, E. Bothe, F. Neese, T. Weyhermüller, K. Wieghardt, *J. Am. Chem. Soc.* **2003**, *125*, 9116–9128; c) E. Bill, E. Bothe, P. Chaudhuri, K. Chlopek, D. Herebian, S. Kokatam, K. Ray, T. Weyhermüller, F. Neese, K. Wieghardt, *Chem. Eur. J.* **2005**, *11*, 204–224; d) K. Chłopek, E. Bill, T. Weyhermüller, K. Wieghardt, *Inorg. Chem.* **2005**, *44*, 7087–7098; e) K. Chłopek, E. Bothe, F. Neese, T. Weyhermüller, K. Wieghardt, *Inorg. Chem.* **2006**, *45*, 6298–6307; f) K. M. Clark, J. Bendix, A. F. Heyduk, J. W. Ziller, *Inorg. Chem.* **2012**, *51*, 7457–7459; g) N. Leconte, J. Ciccione, G. Gellon, C. Philouze, F. Thomas, *Chem. Commun.* **2014**, *50*, 1918–1920; h) J. Ciccione, N. Leconte, D. Luneau, C. Philouze, F. Thomas, *Inorg. Chem.* **2016**, *55*, 649–665; i) K. D. Spielvogel, E. J. Coughlin, H. Petras, J. A. Luna, A. Benson, C. M. Donahue, A. Kibasa, K. Lee, R. Salacinski, S. C. Bart, S. K. Shaw, J. J. Shepherd, S. R. Daly, *Inorg. Chem.* **2019**, *58*, 12756–12774.

[11] a) F. Michel, F. Thomas, S. Hamman, E. Saint-Aman, C. Bucher, J.-L. Pierre, *Chem. Eur. J.* **2004**, *10*, 4115–4125; b) F. Michel, S. Torelli, F. Thomas, C. Duboc, C. Philouze, C. Belle, S. Hamman, E. Saint-Aman, J.-L. Pierre, *Angew. Chem. Int. Ed.* **2005**, *44*, 438–441; *Angew. Chem.* **2005**, *117*, 442; c) S. Gentil, D. Serre, C. Philouze, M. Holzinger, F. Thomas, A. Le Goff, *Angew. Chem. Int. Ed.* **2016**, *55*, 2517–2520; *Angew. Chem.* **2016**, *128*, 2563; d) S. Torelli, C. Belle, I. Gautier-Luneau, J. L. Pierre, E. Saint-Aman, J. M. Latour, L. Le Pape, D. Luneau, *Inorg. Chem.* **2000**, *39*, 3526–3536.

[12] F. Neese, *J. Biol. Inorg. Chem.* **2006**, *11*, 702–711.

[13] N. Hakulinen, J. Rouvinen, *Cell Mol. Life Sci.* **2015**, *72*, 857–868.

[14] B. Reuillard, A. Le Goff, M. Holzinger, S. Cosnier, *J. Mater. Chem. B* **2014**, *2*, 2228–2232.

[15] B. Reuillard, S. Gentil, M. Carrière, A. Le Goff, S. Cosnier, *Chem. Sci.* **2015**, *6*, 5139–5143.

[16] B. Reuillard, K. H. Ly, P. Hildebrandt, L. J. C. Jeuken, J. N. Butt, E. Reisner, *J. Am. Chem. Soc.* **2017**, *139*, 3324–3327.

[17] Y. Yamada, S. Yoshida, T. Honda, S. Fukuzumi, *Energy Environ. Sci.* **2011**, *4*, 2822–2825.

[18] S. Gentil, J. K. Molloy, M. Carrière, A. Hobballah, A. Dutta, S. Cosnier, W. J. Shaw, G. Gellon, C. Belle, V. Artero, F. Thomas, A. Le Goff, *Joule* **2019**, *3*, 2020–2029.

[19] S. Stoll, A. Schweiger, *J. Magn. Reson.* **2006**, *178*, 42–55.

[20] O. V. Dolomanov, L. J. Bourhis, R. J. Gildea, J. A. K. Howard, H. Puschmann, *J. Appl. Crystallogr.* **2009**, *42*, 339–340.

[21] M. J. Frisch, G. W. Trucks, H. B. Schlegel, G. E. Scuseria, M. A. Robb, J. R. Cheeseman, G. Scalmani, V. Barone, B. Mennucci, G. A. Petersson, H. Nakatsuji, M. Caricato, X. Li, H. P. Hratchian, A. F. Izmaylov, J. Bloino, G. Zheng, J. L. Sonnenberg, M. Hada, M. Ehara, K. Toyota, R. Fukuda, J. Hasegawa, M. Ishida, T. Nakajima, Y. Honda, O. Kitao, H. Nakai, T. Vreven, J. A. Montgomery Jr., J. E. Peralta, F. Ogliaro, M. Bearpark, J. J. Heyd, E. Brothers, K. N. Kudin, V. N. Staroverov, R. Kobayashi, J. Normand, K. Raghavachari, A. Rendell, J. C. Burant, S. S. Iyengar, J. Tomasi, M. Cossi, N. Rega, J. M. Millam, M. Klene, J. E. Knox, J. B. Cross, V. Bakken, C. Adamo, J. Jaramillo, R. Gomperts, R. E. Stratmann, O. Yazyev, A. J. Austin, R. Cammi, C. Pomelli, J. W. Ochterski, R. L. Martin, K. Morokuma, V. G. Zakrzewski, G. A. Voth, P. Salvador, J. J. Dannenberg, S. Dapprich, A. D. Daniels, Ö. Farkas, J. B. Foresman, J. V. Ortiz, J. Cioslowski, D. J. Fox, *Gaussian 09, Revision D.01, Gaussian, Inc., Wallingford CT,* ***2009***.

[22] a) J. Tao, J. P. Perdew, V. N. Staroverov, G. E. Scuseria, *Phys. Rev. Lett.* **2003**, *91*, 146401; b) V. N. Staroverov, G. E. Scuseria, J. Tao, J. P. Perdew, *J. Chem. Phys.* **2003**, *119*, 12129–12137.

[23] G. A. Petersson, M. A. Al-Laham, *J. Chem. Phys.* **1991**, *94*, 6081–6090.

[24] M. E. Casida in "Recent Advances in Density Functional Methods" (Ed.: D. P. Chong), World Scientific, Singapore, **1995**.

[25] S. Miertuš, E. Scrocco, J. Tomasi, *Chem. Phys.* **1981**, *55*, 117–129.

Received: April 20, 2020

